Photophysical and photochemical insights of the photodegradation of norfloxacin: The rate-limiting step and the influence of Ca^{2+} ion
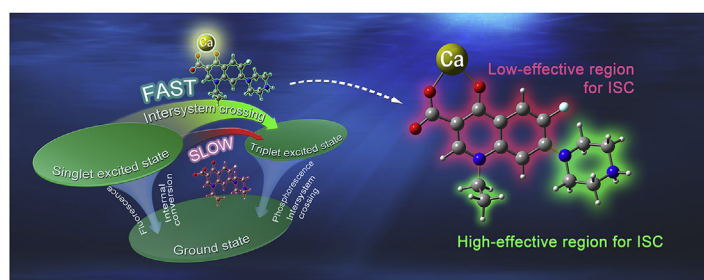
Heming Zhang, Xuedan Song[*], Jianhui Liu, Ce Hao

State Key Laboratory of Fine Chemicals, Dalian University of Technology, Dalian 116024, China

HIGHLIGHTS

- Comprehensively studied photo-physical and photochemical processes of Norfloxacin.
- Identified intersystem crossing as the rate-limiting step of photodegradation.
- Enhanced photophysical characteristics by Ca^{2+} ion.
- Theoretical exploration under the framework of Fermi Golden rule.

GRAPHICAL ABSTRACT

ABSTRACT

Photodegradation is one of the major degradation paths for antibiotics as aquatic micropollutants in surface water. The photodegradation involves a number of complicated photophysical and photochemical processes. Exploration for the rate-limiting step among these processes can be essential for the elimination of antibiotics. In this work norfloxacin was selected as a target compound. The rate constants of photophysical transitions and their competitions were discussed under the framework of Fermi Golden rule and time-depended perturbation theory. Using density functional theory, the reaction paths in triplet state were searched. The competitions among the photophysical transitions and photochemical reaction paths indicate the intersystem crossing (ISC) from the S$_1$ state to T$_1$ state is the rate-limiting step in the aquatic photodegradation of norfloxacin. Ca^{2+} ion significantly accelerates this bottleneck by coordinating with the carbonyl and carboxyl groups of norfloxacin. The coordination creates more ISC paths to triplet states and increases the spin-orbit coupling, Huang-Rhys factors, and the vibrational coupling of the ISCs.

© 2018 Elsevier Ltd. All rights reserved.

1. Introduction

Antibiotics have received increasing concern as the aquatic micro-pollutants in the past decade because of their potential threat to human health and ecological environment (Hughes et al., 2013; Segura et al., 2009). Nowadays, the occurrence of antibiotics is widespread in aquatic environment due to the extensive consuming and continuous discharging (Janecko et al., 2016; Zhang et al., 2015). Under long term exposure, signs of bacterial resistance have already been found in the bacteria sampled from various environmental water (Chen et al., 2012; Shah et al., 2012; Stoll et al., 2012). Photodegradation is one of the major abiotic elimination paths for antibiotics in the surface water (Boreen et al., 2005; Boreen et al., 2004; Ge et al., 2010; Zhu et al., 2016). However, the photodegradation is slow (the half-life is usually over 10 h) (Chen

et al., 2012; Stoll et al., 2012) for a number of antibiotics. To massively and rapidly photodegrade antibiotics in water, different light sources, such as visible and UV light sources (Serna-Galvis et al., 2017), were studied. Various photo-catalysts, such as metal oxide semi-conductors (Ding et al., 2017; Zhu et al., 2016) and carbon materials (Qu et al., 2018; Liu et al., 2017), were designed and tested. Many studies tried to evaluate and estimate the behavior of the photodegradation of organic contaminants through analyzing quantitative structure-property relations (Chen et al., 2001; Zeng et al., 2016). Although considerable effort has been made to evaluate and enhance the photodegradation of antibiotics, the fundamental mechanisms were still not fully illustrated. Thus, the slowest step that limits the rate of the overall process of photodegradation is usually unknown. The mechanism of the photodegradation involves complicated photophysical and photochemical processes. To date, mechanisms of the photochemical processes for some antibiotics have been studied by density functional theory (DFT) computation (Tentscher et al., 2013; Wang et al., 2015; Wei et al., 2013; Zeng et al., 2016). However, photophysical processes have been less investigated. Photophysical processes include fluorescence emission (F) and internal conversion (IC) from the first singlet excited (S_1) state to the ground (S_0) state, intersystem crossing (ISC) from the S_1 state to the excited triplet (T_n) states, and phosphorescence emission (P) and ISC from the T_1 state to the S_0 state (when considering Kasha's rule that one photophysical or photochemical process initiates from the lowest lying excited state). Knowing the rate constants of these photophysical transitions is of extraordinary importance because the competitions among these transitions lead the antibiotic molecules to different fates: after the reactant molecules are excited to the S_1 state whether the molecules will preferentially enter the T_1 state or fall back to the S_0 state from the S_1 state, and whether it is more favorable undergoing a photochemical reaction in the T_1 state or returning to the S_0 state from the T_1 state and losing reactivity. Accordingly, the investigation of the photophysical process is important and essential to obtain a comprehensive and complete view of the photodegradation process. After the details of each path of photophysical and photochemical processes become clear, the rate-limiting step can be identified. Then, it is possible to determine the reason that directly limits the rate of the photodegradation.

On the other hand, the water systems are extremely complicated. Many factors have influence on the photodegradation of antibiotics. There are already some good examples that the photodegradation of antibiotics are enhanced in natural water. For instance, Werner et al. (2006) found Ca^{2+} and Mg^{2+}, as two of the most common metal ions in natural water, enhanced the photodegradation of tetracycline. Sturini et al. (2010) reported that Ca^{2+} was able to enhance the photodegradation of several fluoroquinolone antibiotics. It seems that some metal ions serve as the natural photocatalyst in the environmental water. The mechanisms behind the metal ions' influence can be fascinating and motivating for the improvement of photocatalytic elimination of antibiotics in water.

In this work, norfloxacin, which belongs to the fluoroquinolone class of antibiotics, was chosen as a target model because it has been wildly applied in animal agriculture and human medicine as a broad-spectrum antibiotic (Claeys et al., 2018; Golet et al., 2002; Kim et al., 2018). Its concentration was detected in high level in water systems. For instance, in urban sewage the concentration of norfloxacin was reported as 568 ng/l and the concentration was still 73 ng/L after the sewage treatment plant process (Golet et al., 2002). Herein, we explored the photophysical and the photochemical processes of norfloxacin. The photophysical transition rate constants were calculated under the framework of Fermi Golden rule and time-depended perturbation theory. The reaction paths of photochemical process were searched using DFT method. The competitions among these photophysical transitions and photochemical reaction paths were discussed and the rate-limiting step was finally identified. Furthermore, the influence of Ca^{2+} on the rate-limiting step of norfloxacin was investigated.

2. Methodology

2.1. Theory

Under the framework of Fermi Golden rule and Franck-Condon approximation, the radiative transition spectrum is expressed as (Niu et al., 2010; Peng et al., 2007):

$$\sigma_{emi}(\omega, T) = \frac{4\omega^3}{3\hbar c^3} \sum_{u,\nu} P_{i\nu}(T) \left| \left\langle \Theta_{fu} \middle| \boldsymbol{\mu}_{fi} \middle| \Theta_{i\nu} \right\rangle \right|^2 \delta\left(\omega_{i\nu,fu} - \omega\right) \quad (1)$$

where $\hbar$ is reduced Planck constant, ω is circular frequency, i and f represent initial and final states respectively, $\omega_{i\nu,fu}$ is the difference of the frequencies between the initial and the final states, $P_{i\nu}$ is the Boltzmann distribution of initial state, ν and u are the vibrational quantum number of initial and final states respectively, Θ is vibrational wavefunction, $\boldsymbol{\mu}_{fi}$ is the transition dipole moment from initial electronic state $|\Phi_i\rangle$ to final electronic state $|\Phi_f\rangle$.

The rate constant of the radiative transition is obtained by the integration of its spectrum (Niu et al., 2010; Peng et al., 2007):

$$k_r(T) = \int \sigma_{emi}(\omega, T) d\omega \quad (2)$$

Rate constant of IC and ISC as non-radiative transitions are expressed as (Niu et al., 2008; Peng et al., 2013):

$$k_{IC} = \frac{2\pi}{\hbar} \sum_{u,\nu} P_{i\nu}(T) \left| \sum_n \left\langle \Phi_f \middle| \widehat{P}_n \middle| \Phi_i \Theta_{fu} \middle| \widehat{P}_n \middle| \Theta_{i\nu} \right\rangle \right|^2 \delta\left(E_{i\nu} - E_{fu}\right) \quad (3)$$

$$k_{ISC} = \frac{2\pi}{\hbar} \sum_{u,\nu} P_{i\nu}(T) \left| \left\langle \Phi_f \middle| \widehat{H}^{SO} \middle| \Phi_i \right\rangle \right|^2 \left| \left\langle \Theta_{fu} \middle| \Theta_{i\nu} \right\rangle \right|^2 \delta\left(E_{i\nu} - E_{fu}\right) \quad (4)$$

where n is the index of normal vibrational modes in eq. (3), $\widehat{P}_n$ is the momentum operator of the nth normal vibrational mode in final state, $\widehat{H}^{SO}$ is Hamiltonian operator of spin-orbit coupling. $\left| \Phi_f \middle| \widehat{P}_n \middle| \Phi_i \right|^2$ was solved by the computation of transition of electric field (Peng et al., 2013).

2.2. Computational details

Geometry optimization and vibrational frequency were computed by using Gaussian09 package (Frisch et al., 2009). For the S_0 state and the excited states the geometries and vibrational modes were respectively computed by DFT and TD-DFT (Bauernschmitt and Ahlrichs, 1996; Parr and Yang, 1989). The functional of B3LYP (Becke, 1993) and standard 6-311 + G(d,p) basis set (McLean and Chandler, 1980; Raghavachari et al., 1980) were applied. The integral equation formalism of polarized continuum model (IEFPCM) (Tomasi et al., 2005) as the solvent model in Gaussian09 package was selected and the solvent is water. Tight convergence and ultrafine grid-size were applied in the self-consistent field computation. The computation of transition of electric field required by IC was performed at the same level of theory with the computation of geometry optimization and vibrational frequency. The computation of spin-orbit coupling and the phosphorescence transition dipole moment were computed by ADF2013 package (ADF 2013, http://www.scm.com; Fonseca et al.,

1998; te Velde et al., 2001) using scalar zero-order regular approximation (ZORA) (van Lenthe et al., 1993, 1994, 1996a; 1996b, 1999) and TD-DFT on the level of B3LYP/Aug-TZP (Baerends et al., 1973). The rate constants and emission spectrum were calculated by MOMAP program (Niu et al., 2008, 2010; Peng et al., 2007, 2013). In all the computation of transition constants the electronic vibronic couplings (EVC) in the form of internal coordinate were used and the Duschinsky rotation effect was turned off. For the potential energy surfaces in the triplet state unrestricted DFT method was applied. Intrinsic reaction coordinate (IRC) method (Fukui, 1981) was used to confirm paths towards reactant and product linked with a transitional state geometry in an elementary reaction. Zero-point energy correction was considered for each stationary point.

According to the research by Wammer et al. (2013) about the photodegradation of fluoroquinolone antibiotics, typically this classification of antibiotics has several dissociation forms in different pH conditions. For norfloxacin the first pK_a is 6.11 (−COOH) and the second is 9.11 (=NH$_2^+$). Around neutral condition the main form is zwitterion (the structures of different dissociation forms are shown in Fig. 1). Under different pH norfloxacin is stable in dark. Under illumination of xenon lamp the highest photo-degradation rate was observed in a weak alkaline environment (pH = 7.7) (Wammer et al., 2013). Therefore, the geometry of zwitterion form of norfloxacin was chosen in the computation.

2.3. Chemicals and emission spectrum measurement

Norfloxacin (98%) was purchased from Aladdin industrial corporation, Co., Ltd. in Shanghai. Fluorescence luminescence spectrum of norfloxacin was measured by Thermo Scientific Lumina spectrophotometer using a quartz cuvette. The slit was 5 nm. The excitation wavelength was 340 nm which was selected according to the excitation spectrum of norfloxacin measured.

3. Results and discussion

3.1. Competition in S$_1$ state

As shown in Fig. 2(a) there are three competing transition paths in the S$_1$ state: The F, the IC, and the ISC (S$_1$→T$_1$). The corresponding rate constants (k_F, k_{IC}, and $k_{ISC\,(S1→T1)}$) were calculated and shown in Fig. 2(b). The IC is the largest one among the three ($k_{IC} = 6.20 \times 10^8/s^{-1}$. The experimental value of the k_{IC} is $3.70 \times 10^8/s^{-1}$ (Park et al., 2002)). The k_F calculated as $3.51 \times 10^7/s^{-1}$ (The experimental value of k_F is $6.48 \times 10^7/s^{-1}$ (Park et al., 2002)) is less than one order of magnitude lower than the k_{IC}. The difference between the calculated and experimental values of rate constant is within one order of magnitude, which means the calculated results are reasonable. The ISC (S$_1$→T$_1$) is the slowest one among the three transitions, as shown in Fig. 2(b). Its rate constant ($k_{ISC\,(S1→T1)} = 4.57 \times 10/s^{-1}$) is about 7 and 6 orders of magnitude lower than the k_{IC} and the k_F respectively, meaning the majority of the norfloxacin molecules in the S$_1$ state tend to return to the S$_0$ state from the S$_1$ state and only a small proportion of them is able to reach the T$_1$ state. It is disadvantageous for the reactions to take place in the T$_1$ state in the next step. The ISC (S$_1$→T$_1$) is probably the bottleneck in the photophysical processes. The computed fluorescence emission transition electric dipole moment is 3.1 Debye which means the fluorescence luminescence is dipole allowed. The calculated fluorescence spectrum (as shown in Fig. S1) is coherent with the experimentally measured result, which means the theoretical method and the calculated results are reasonable.

3.2. Competition in T$_1$ state

After norfloxacin molecules arrive in the T$_1$ state they can fall back to S$_0$ state through the phosphorescence emission and the ISC (T$_1$→S$_0$), or continue to undergo the photo-reactions as shown in Fig. 2(a) and (c). The rate constants of the phosphorescence and the ISC (T$_1$→S$_0$) (k_P and $k_{ISC\,(T1→S0)}$) were shown in Fig. 2(b). Both the k_P and the $k_{ISC\,(T1→S0)}$ are small, meaning a long lifetime in the T$_1$ state before norfloxacin molecules return to the S$_0$ state. This conclusion is coherent with the recent experimental findings by Niu et al. (2018). Meanwhile, the small value of the k_P may imply weak luminescence intensity. At room temperature the phosphorescence emission of norfloxacin was not detectable in this study.

In order to investigate the competition in the T$_1$ state, the rate constants of photo-reactions are studied. As discussed above, the ISC (S$_1$→T$_1$) is probably the bottleneck due to its low rate constant. We need to find out if there is a reaction path that is faster than the ISC (S$_1$→T$_1$) to identify the rate-limiting step of the overall process of the photodegradation. If none of the reaction paths is faster than the ISC (S$_1$→T$_1$), then the photodegradation of norfloxacin is actually limited by the photochemical process rather than the ISC (S$_1$→T$_1$); if one or several reaction paths are found faster than ISC (S$_1$→T$_1$), it will be clear that the ISC (S$_1$→T$_1$) is the rate-limiting step. According to the experimental research on the photolysis of fluoroquinolones (Ge et al., 2010; Liang et al., 2015; Wei et al., 2013; Zhang et al., 2019), several representative reaction paths were schemed and calculated by unrestricted DFT method. The paths included substitution of the −F by the −OH, decarboxylation, and cleavage of the piperazine ring. More information of the representative photo-reactions of norfloxacin were discussed in the supporting information (see Fig. S2).

The possible reaction paths and the corresponding activation energies (E_as) are depicted in Fig. 2(c). Path-1 is the reaction path with the lowest E_a (4.9 kcal mol^{-1}). The −F group is substituted by the HO$^-$ and the F$^-$ ion is produced (the distance between the F atom and the C atom is finally stretched to 4.27 Å, as shown in Fig. 2(c)). For Path-2, the carboxyl group is eliminated and CO$_2$ is produced (the length of the C−O bond is stretched from 1.53 Å to 3.48 Å). The E_a of this path is 28.6 kcal mol^{-1} that is the highest E_a of all the calculated paths. In Path-3 and 4, the reaction starts from the structure in which the piperazine is protonated. In Path-3, the piperazine ring cleavages with an E_a of 9.3 kcal mol^{-1} (the C−N in the piperazine ring is stretched to 3.22 Å). Then the dihedral of C−N−C−C rotates to another conformation of lower energy with an E_a of 0.6 kcal mol^{-1}. In Path-4, the piperazine is separated when the distance between the C atom and the N atom increases (the length of the C−N bond is stretched from 1.47 Å to 2.45 Å) with an E_a of 11.2 kcal mol^{-1}. A piperazine-exclusion intermediate is produced. Then, piperazine-exclusion intermediate joints a hydroxyl ion to
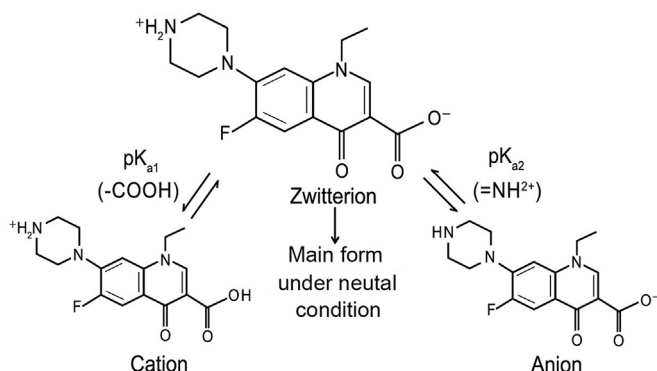

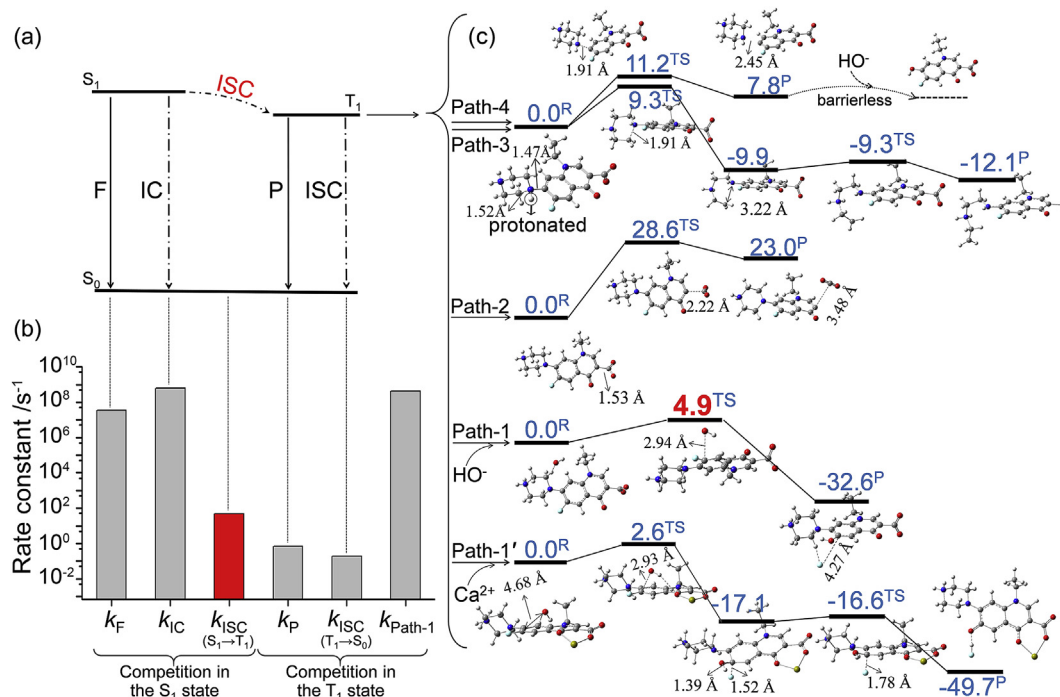**Fig. 1.** Different dissociation forms of norfloxacin in water.

Fig. 2. Photophysical and photochemical processes of the photodegradation of norfloxacin. (a) The photophysical transitions of norfloxacin. F: fluorescence emission, IC: internal conversion, ISC: intersystem crossing, P: phosphorescence emission. (b) Rate constants of the photophysical transitions and the reaction path with the lowest activation energy (Path-1). (c) The possible reaction paths and the corresponding activation energies. The blue number on each stationary point is the relative energy in the unit of kcal/mol. R: reactant, TS: transition state, P: product. Carbon: gray, nitrogen: blue, fluorine: cyan, oxygen: red, calcium: yellow. (For interpretation of the references to colour in this figure legend, the reader is referred to the Web version of this article.)

generate the final product of this reaction path (this reaction is barrierless in the S_0 state). Therefore, Path-1 is the path with the lowest activation energy when comparing the E_as of these reaction paths. Its rate constant is used to evaluate the rate constant of the photochemical process. The reaction rate constant of Path-1 is calculated with the transition state theory (Eyring, 1935):

$$k_R = \kappa_i \frac{k_B T}{h} \exp\left(-\frac{\Delta G^{\ddagger}}{RT}\right) \qquad (5)$$

where k_B and h are Boltzmann and Planck constants, respectively; $\Delta G^{\ddagger}$ is the activation free energy which is the difference of the free energies between the transition state and the reactant of one elementary reaction. The $\Delta G^{\ddagger}$ of the Path-1 is calculated to be 23857.9 J/mol; κ_i is transmission coefficient which was calculated by the following equation (Louis et al., 2000):

$$\kappa_i = 1 + \frac{1}{24}\left(\frac{h\nu_i}{k_B T}\right)^2 \qquad (6)$$

where ν_i is the imaginary frequency of transition state. The calculated reaction rate constant of Path-1 is $4.10 \times 10^8/s^{-1}$.

Then, we have all the rate constants of the phosphorescence emission, the ISC ($T_1 \rightarrow S_0$), and the reaction Path-1 as three competing processes in the T_1 state. As shown in Fig. 2(b) it is evident that the reaction of Path-1 in the T_1 state is much faster than the phosphorescence emission and the ISC ($T_1 \rightarrow S_0$). After norfloxacin molecules arrive in the T_1 state they will easily undergo the reaction of Path-1, rather than fall to the S_0 state from the T_1 state through the phosphorescence emission and the ISC ($T_1 \rightarrow S_0$). Comparing the rate constants of ISC ($S_1 \rightarrow T_1$) and that of the Path-1, it is clear that the ISC ($S_1 \rightarrow T_1$) is slower than the reaction of Path-1 in the T_1 state. Thus, the ISC ($S_1 \rightarrow T_1$) is finally identified as the rate-

limiting step in the photodegradation of norfloxacin. The key to enhance the photodegradation of norfloxacin is to increase the rate of the ISC ($S_1 \rightarrow T_1$).

3.3. The influence of Ca^{2+} on ISC

Sturini et al. (2010) reported that several common ions in natural water, including Ca^{2+}, Mg^{2+}, Cl^-, and PO_4^{3-}, had different effects on the photodegradation of fluoroquinolones. Among them, Ca^{2+} ion was able to increase the photodegradation rate constant of several fluoroquinolones. It is a good example in natural water to help us understand the mechanism that the photodegradation is enhanced. Herein, we focused on the effect of Ca^{2+} on the ISC ($S_1 \rightarrow T_1$) because, as mentioned above, the ISC ($S_1 \rightarrow T_1$) is the rate-limiting step. The oxygen-containing functional groups, namely carbonyl and carboxyl groups, of norfloxacin are able to form complexes with the Ca^{2+} ion (NOR-Ca complexes). Among the models of the complexes (see Fig. 3), the most stable one is the complex with the coordination between the Ca^{2+} ion and the oxygen atoms in the carbonyl and carboxyl groups (in Fig. 3(a)). This is coherent with the experimental findings (Turel, 2002). Thus, this model was chosen in the following studies. It is true that the metal ion complex in a real water system is rather complex considering the hydrogen bond framework and many other factors. While, we are interested in determining the foremost characteristic of the effect induced by the Ca^{2+} ion. Herein, the simplified model was adopted with one Ca^{2+} ion and the solvent model of water.

Based upon the optimized geometry of the S_1 state the vertical energies towards different triplet states and the corresponding spin-orbit coupling constants were computed and listed in Table 1. For NOR-Ca complex there are four triplet states (T_1, T_2, T_3, and T_4) lying lower than the S_1 state (vertical energy). The ISC from the S_1 state to any of these triplet states can occur. For norfloxacin
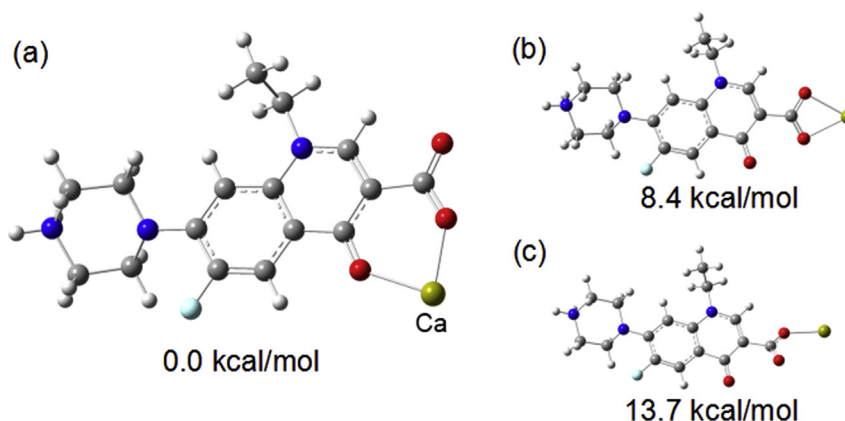
Fig. 3. The structures and relative energies of the complexes formed between the norfloxacin molecule and the Ca^{2+} ion. The Ca^{2+} ion is coordinated with (a) the oxygen atoms in the carbonyl and carboxyl groups, (b) the two oxygen atoms in the carboxyl group, or (c) one single oxygen atom in the carboxyl group. Carbon: gray, nitrogen: blue, fluorine: cyan, oxygen: red, calcium: yellow. (For interpretation of the references to colour in this figure legend, the reader is referred to the Web version of this article.)

monomer only the energy of T_1 state is lower than that of the corresponding S_1 state. Thus, there are more transition channels of ISCs for the NOR-Ca complex, which is helpful for the NOR-Ca complex to enter the triplet state through the ISCs. The spin-orbit coupling constants (H^{SO}) for the NOR-Ca complex from the S_1 state to the T_1, T_2, T_3, and T_4 states were computed (in Table 1). The ISCs from the S_1 state to the T_3 and T_4 states have two largest H^{SO}s. The values of these two H^{SO}s are several orders of magnitude higher than the H^{SO} of the ISC ($S_1 \rightarrow T_1$) for the norfloxacin monomer. Thus, the coordination with the Ca^{2+} ion significantly increases the spin-orbit coupling, which is favorable for the NOR-Ca complex to enter the triplet state. We calculated the ISC rate constants of the NOR-Ca complex from the S_1 state to the T_3 and T_4 states as two representative ISCs. As shown in Table 1, the rate constants of the ISC ($S_1 \rightarrow T_3$) and the ISC ($S_1 \rightarrow T_4$) of the NOR-Ca complex are $2.73 \times 10^{10} \, s^{-1}$ and $3.37 \times 10^9 \, s^{-1}$ respectively. They are several orders of magnitude larger than the rate constant of the ISC ($S_1 \rightarrow T_1$) of the norfloxacin monomer, implying that the Ca^{2+} ion can effectively enhance the ISC to bring the complex into the triplet state. It is important to note that in the real water system the photodegradation rate constant of fluoroquinolones cannot be increased that much (Sturini et al., 2010) due to the low coordination constant (Kawai et al., 1996).

Additionally, we also calculated the rate constants of the IC and the fluorescence emission of the NOR-Ca complex. The k_{IC} for the NOR-Ca complex was calculated to be $6.18 \times 10^7 \, s^{-1}$ and it is about one order of magnitude lower than that of the norfloxacin monomer ($6.20 \times 10^8 \, s^{-1}$). The k_F for the NOR-Ca complex is $1.02 \times 10^8 \, s^{-1}$, which is less than one order of magnitude higher than that of the norfloxacin monomer ($3.51 \times 10^7 \, s^{-1}$). Generally, the sum of the rate constants of the IC and the fluorescence

emission, which represents the total rate constant that the system fall to the S_0 state from the S_1 state, is not significantly changed under the influence of Ca^{2+} ion.

Noteworthy, not only the Ca^{2+} ion is able to change the electronic property of norfloxacin, but also it has influence on the coupling of vibrational modes from the initial state to the final state. The vibrational coupling between the initial state and the final state is described by the Franck-Condon factor $\left| \Theta_{fu} | \Theta_{iv} \right|^2$ in Eq. (4). It can be expressed by the Huang-Rhys factor and displacement harmonic oscillator (Peng et al., 2007):

$$\left| \left\langle \Theta_{fu} | \Theta_{iv} \right\rangle \right|^2 = \prod_k \left| \left\langle \chi_{fu_k} | \chi_{iv_k} \right\rangle \right|^2 = \frac{S_k^{u_k}}{u_k!} e^{-S_k} \tag{7}$$

where χ is displacement harmonic oscillator, S is Huang-Rhys factor, u_k is the kth vibrational mode in final state of transition. Therefore, the contribution of a certain vibrational mode to the vibrational coupling is described by its Huang-Rhys factor. The vibrational modes and their Huang-Rhys factors of the final states in the ISCs of the NOR-Ca complex and the norfloxacin monomer are shown in Fig. 4. It is evident that the Huang-Rhys factors in the ISC ($S_1 \rightarrow T_3$) and ISC ($S_1 \rightarrow T_4$) of the NOR-Ca complex (in Fig. 4(b) and (c)) are much larger than that of the ISC ($S_1 \rightarrow T_1$) of the norfloxacin monomer (in Fig. 4(a)). This means much stronger coupling of the vibrational modes of the NOR-Ca complex in the processes of the ISCs. The largest Huang-Rhys factor for norfloxacin monomer is not more than 0.16 (in Fig. 4(a)), which means the vibrational coupling is weak in the ISC ($S_1 \rightarrow T_1$). Comparatively, the largest Huang-Rhys factor are over 5 for the ISC ($S_1 \rightarrow T_3$) and ISC ($S_1 \rightarrow T_4$) of the NOR-Ca complex in Fig. 4(b) and (c). In addition, the vibrational modes, that make the major contribution, move from about $700 \, cm^{-1}$ to lower than $100 \, cm^{-1}$ (low frequency region) after the complex is formed compared with the norfloxacin monomer. This may result in more quantum numbers of transition and increase the rate constant of a non-radiative transition (Peng et al., 2007; Zhang et al., 2014). Furthermore, the vibrational displacement (the small blue arrows extend from the atoms in Fig. 4) of the mode that has the largest Huang-Rhys factor for the ISC ($S_1 \rightarrow T_1$) of norfloxacin monomer is distributed throughout the whole molecule in Fig. 4(a). In contrast, for the ISC ($S_1 \rightarrow T_3$) and the ISC ($S_1 \rightarrow T_4$) (in Fig. 4(b) and (c)) of the NOR-Ca complex the vibrational displacements of the modes which have the largest Huang-Rhys factors are mostly concentrated on the piperazine ring and the ethyl group. That means that the vibrations of the piperazine ring and the ethyl group

Table 1
Vertical excitation energies (ΔE_{vert}) from the S_1 state (as the reference state) to each of the excited triplet states, the corresponding spin-orbit coupling constants, and the rate constants. Negative value of ΔE_{vert} means the energy of the final state is lower than that of the initial state.

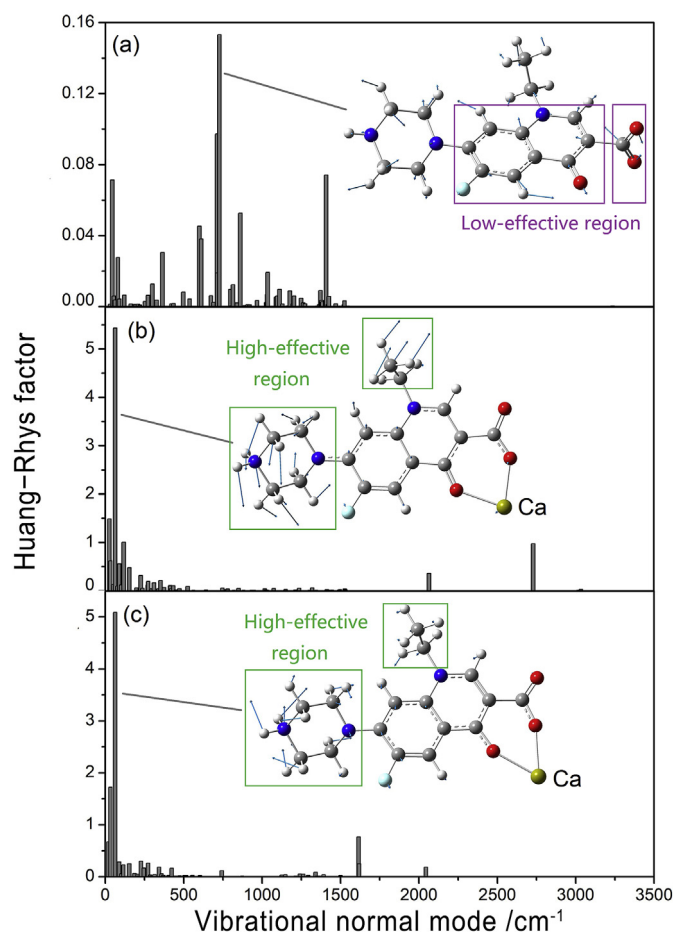|	ISC	ΔE_{vert}/eV	H^{SO}/cm^{-1}	Rate constant/s^{-1}
NOR-Ca^{2+} complex	$S_1 \rightarrow T_1$	−1.54	3.63	—
	$S_1 \rightarrow T_2$	−1.37	2.05	—
	$S_1 \rightarrow T_3$	−0.99	20.31	2.73×10^{10}
	$S_1 \rightarrow T_4$	−0.36	15.70	3.37×10^9
	$S_1 \rightarrow T_5$	0.30	—	—
Norfloxacin	$S_1 \rightarrow T_1$	−0.08	0.018	4.57×10
	$S_1 \rightarrow T_2$	0.58	—	—

Fig. 4. Huang-Rhys factors and vibrational modes of the final states in (a) the ISC ($S_1 \rightarrow T_1$) of the norfloxacin monomer, (b) the ISC ($S_1 \rightarrow T_3$) of the NOR-Ca complex, and (c) the ISC ($S_1 \rightarrow T_4$) of the NOR-Ca complex. The blue arrows extended from the atoms are the displacement vectors of a vibrational mode. Carbon: gray, nitrogen: blue, fluorine: cyan, oxygen: red, calcium: yellow. (For interpretation of the references to colour in this figure legend, the reader is referred to the Web version of this article.)

contribute most to the ISC. Comparing the vibrational modes in Fig. 4(b) and (c) with that in Fig. 4(a), it is obvious that the vibrational displacements in the carboxyl group and the nearby region are inhibited after the coordination with the Ca^{2+} ion. The reason may be that the coordination between the Ca^{2+} and the oxygen-containing groups makes carboxyl group and the nearby region more rigid (without the coordination with the Ca^{2+} the carboxyl group is flexible and it can rotate through the C—C single bond). This may inhibit the vibrations of carboxyl group. In another word, the vibrations of the carboxyl group may be ineffective in the ISC transition. The inhibition of the vibrations in this region is possibly beneficial for ISC. The vibrations of the piperazine ring and the ethyl group, by contrast, are highly responsible for the ISC transitions. The Ca^{2+} ion makes the vibrational displacements mostly concentrated on these two functional groups and consequently makes the ISC transitions more efficient. Similar conclusion can also be drawn for the initial states of the ISCs of the NOR-Ca complex and the norfloxacin monomer (shown in Fig. S3). More details of the vibrational couplings were discussed in the SI.

Additionally, Ca^{2+} ion also reduces the activation energy of Path-1 to 2.6 kcal mol^{-1} (as shown in Path-1' in Fig. 2(c)). The original one-step reaction in Path-1 is changed into two steps as shown in Path-1'. The decrease of the activation energy makes this photo-reaction faster, which is also beneficial for the photodegradation.

4. Conclusion

Through the systematic investigation of the photophysical and photochemical processes, it is established that the ISC transition from the S_1 state to the T_1 state is the rate-limiting step in the photodegradation of norfloxacin. It is a new perspective that a photophysical transition is identified as the rate-limiting step of the photodegradation process. The study of photophysical processes is important and essential to have a comprehensive view of the photodegradation. Ca^{2+} ion can coordinate with the carbonyl and carboxyl groups of norfloxacin and enhance the rate-limiting step. Ca^{2+} ion has influence on several photophysical properties of norfloxacin, including the spin-orbit coupling, Huang-Rhys factors, and vibrational couplings. This is a new understanding about how a common metal ion in water exerts influence on the photodegradation of an antibiotic through improving the photophysical properties. We hope the basic understandings of photophysical and photochemical processes and the rate-limiting step in this research will provide theoretical supports for the efficient elimination of antibiotics.

Appendix A. Supplementary data

Supplementary data to this article can be found online at https://doi.org/10.1016/j.chemosphere.2018.11.198.

References

ADF2013, SCM, Theoretical Chemistry, Vrije Universiteit, Amsterdam, the Netherlands, http://www.scm.com;

Baerends, E.J., Ellis, D.E., Ros, P., 1973. Self-consistent molecular Hartree-Fock-Slater calculations I. the computational procedure. Chem. Phys. 2 (1), 41–51. https://doi.org/10.1016/0301-0104(73)80059-X.

Bauernschmitt, R., Ahlrichs, R., 1996. Treatment of electronic excitations within the adiabatic approximation of time dependent density functional theory. Chem. Phys. Lett. 256 (4–5), 454–464. https://doi.org/10.1016/0009-2614(96)00440-X.

Becke, A.D., 1993. Density-functional thermochemistry. III. the role of exact exchange. J. Chem. Phys. 98 (7), 5648–5652. https://doi.org/10.1063/1.464913.

Boreen, A.L., Arnold, W.A., McNeill, K., 2004. Photochemical fate of sulfa drugs in the aquatic environment: sulfa drugs containing five-membered heterocyclic groups. Environ. Sci. Technol. 38 (14), 3933–3940. https://doi.org/10.1021/es0353053.

Boreen, A.L., Arnold, W.A., McNeill, K., 2005. Triplet-sensitized photodegradation of sulfa drugs containing six-membered heterocyclic groups: identification of an SO$_2$ extrusion photoproduct. Environ. Sci. Technol. 39 (10), 3630–3638. https://doi.org/10.1021/es048331p.

Chen, J., Jin, M., Qiu, Z.G., Guo, C., Chen, Z.L., Shen, Z.Q., Wang, X.W., Li, J.W.A., 2012. Survey of drug resistance bla genes originating from synthetic plasmid vectors in six Chinese rivers. Environ. Sci. Technol. 46 (24), 13448–13454. https://doi.org/10.1021/es302760s.

Chen, J., Quan, X., Peijnenburg, W.J.G.M., Yang, F., 2001. Quantitative structure-property relationships (QSPRs) on direct photolysis quantum yields of PCDDs. Chemosphere 43 (2), 235–241. https://doi.org/10.1016/S0045-6535(00)00141-7.

Claeys, K.C., Hopkins, T.L., Vega, A.D., Heil, E.L., 2018. Fluoroquinolone restriction as an effective antimicrobial stewardship intervention. Curr. Infect. Dis. Rep. 20 (5), 7. https://doi.org/10.1007/s11908-018-0615-z.

Ding, J., Dai, Z., Qin, F., Zhao, H., Zhao, S., Chen, R., 2017. Z-scheme BiO1-xBr/Bi$_2$O$_2$CO$_3$ photocatalyst with rich oxygen vacancy as electron mediator for highly efficient degradation of antibiotics. Appl. Catal., B 205, 281–291. https://doi.org/10.1016/j.apcatb.2016.12.018.

Eyring, H., 1935. The activated complex in chemical reactions. J. Chem. Phys. 3, 107–115.

Fonseca, G.C., Snijders, J.G., te Velde, G., Baerends, E.J., 1998. Towards an order-N DFT method. Theor. Chem. Acc. 99 (6), 391–403. https://doi.org/10.1007/s002140050021.

Frisch, M.J., Trucks, G.W., Schlegel, H.B., Scuseria, G.E., Robb, M.A., Cheeseman, J.R., Scalmani, G., Barone, V., Mennucci, B., Petersson, G.A., Nakatsuji, H., Caricato, M., Li, X., Hratchian, H.P., Izmaylov, A.F., Bloino, J., Zheng, G., Sonnenberg, J.L., Hada, M., Ehara, M., Toyota, K., Fukuda, R., Hasegawa, J., Ishida, M., Nakajima, T., Honda, Y., Kitao, O., Nakai, H., Vreven, T., Montgomery, J.J.A., Peralta, J.E., Ogliaro, F., Bearpark, M., Heyd, J.J., Brothers, E., Kudin, K.N., Staroverov, V.N., Kobayashi, R., Normand, J., Raghavachari, K., Rendell, A., Burant, J.C., Iyengar, S.S., Tomasi, J., Cossi, M., Rega, N., Millam, J.M., Klene, M., Knox, J.E., Cross, J.B., Bakken, V., Adamo, C., Jaramillo, J., Gomperts, R., Stratmann, R.E., Yazyev, O., Austin, A.J., Cammi, R., Pomelli, C., Ochterski, J.W., Martin, R.L., Morokuma, K., Zakrzewski, V.G., Voth, G.A., Salvador, P., Dannenberg, J.J., Dapprich, S., Daniels, A.D., Farkas, Ö., Foresman, J.B., Ortiz, J.V., Cioslowski, J., Fox, D.J., 2009. Gaussian. Gaussian Inc., Wallingford, CT.

Fukui, K., 1981. The path of chemical-reactions - the IRC approach. Acc. Chem. Res. 14 (12), 363—368. https://doi.org/10.1021/ar00072a001.

Ge, L., Chen, J., Wei, X., Zhang, S., Qiao, X., Cai, X., Xie, Q., 2010. Aquatic photochemistry of fluoroquinolone antibiotics: kinetics, pathways, and multivariate effects of main water constituents. Environ. Sci. Technol. 44 (7), 2400—2405. https://doi.org/10.1021/es902852v.

Golet, E.M., Alder, A.C., Giger, W., 2002. Environmental exposure and risk assessment of fluoroquinolone antibacterial agents in wastewater and river water of the Glatt Valley watershed, Switzerland. Environ. Sci. Technol. 36 (17), 3645—3651. https://doi.org/10.1021/es0256212.

Hughes, S.R., Kay, P., Brown, L.E., 2013. Global synthesis and critical evaluation of pharmaceutical data sets collected from river systems. Environ. Sci. Technol. 47 (2), 661—677. https://doi.org/10.1021/es3030148.

Janecko, N., Pokludova, L., Blahova, J., Svobodova, Z., Literak, I., 2016. Implications of fluoroquinolone contamination for the aquatic environment-a review. Environ. Toxicol. Chem. 35 (11), 2647—2656. https://doi.org/10.1002/etc.3552.

Kawai, Y., Matsubayashi, K., Hakusui, H., 1996. Interaction of quinolones with metal cations in aqueous solution. Chem. Pharm. Bull. 44 (8), 1425—1430.

Kim, C., Ryu, H.-D., Chung, E.G., Kim, Y., Lee, J.K., 2018. A review of analytical procedures for the simultaneous determination of medically important veterinary antibiotics in environmental water: sample preparation, liquid chromatography, and mass spectrometry. J. Environ. Manag. 217, 629—645. https://doi.org/10.1016/j.jenvman.2018.04.006.

Liu, J.Y., Song, Y.H., Xu, H., Zhu, X.W., Lian, J.B., Xu, Y., Zhao, Y., Huang, L.Y., Ji, H.Y., Li, H.M., 2017. Non-metal photocatalyst nitrogen-doped carbon nanotubes modified mpg-C3N4: facile synthesis and the enhanced visible-light photocatalytic activity. J. Colloid Interface Sci. 494, 38—46. https://doi.org/10.1016/j.jcis.2017.01.010.

Liang, C., Zhao, H.M., Deng, M.J., Quan, X., Chen, S., Wang, H., 2015. Impact of dissolved organic matter on the photolysis of the ionizable antibiotic norfloxacin. J. Envion. Sci. 27, 115—123. https://doi.org/10.1016/j.jes.2014.08.015.

Louis, F., Gonzalez, C.A., Huie, R.E., 2000. An ab initio study of the kinetics of the reactions of halomethanes with the hydroxyl radical. 1. CH2Br2. J. Phys. Chem. 104 (13), 2931—2938. https://doi.org/10.1021/jp991022e.

McLean, A.D., Chandler, G.S., 1980. Contracted Gaussian-basis sets for molecular calculations. 1. 2nd row atoms, Z=11-18. J. Chem. Phys. 72 (10), 5639—5648. https://doi.org/10.1063/1.438980.

Niu, X.Z., Moore, E.G., Croué, J.-P., 2018. Excited triplet state interactions of fluoroquinolone norfloxacin with natural organic matter: a laser spectroscopy study. Environ. Sci. Technol. 53 (18), 10426—10432. https://doi.org/10.1021/acs.est.8b02835.

Niu, Y., Peng, Q., Deng, C., Gao, X., Shuai, Z.G., 2010. Theory of excited state decays and optical spectra: application to polyatomic molecules. J. Phys. Chem. 114 (30), 7817—7831. https://doi.org/10.1021/jp101568f.

Niu, Y., Peng, Q., Shuai, Z.G., 2008. Promoting-mode free formalism for excited state radiationless decay process with Duschinsky rotation effect. Sci. China, Ser. B 51 (12), 1153—1158. https://doi.org/10.1007/s11426-008-0130-4.

Park, H.-R., Kim, T.H., Bark, K.-M., 2002. Physicochemical properties of quinolone antibiotics in various environments. Eur. J. Med. Chem. 37 (6), 443—460. https://doi.org/10.1016/S0223-5234(02)01361-2.

Parr, R.G., Yang, W., 1989. Density-functional Theory of Atoms and Molecules. Oxford Univ. Press, Oxford.

Peng, Q., Niu, Y., Shi, Q., 2013. Correlation function formalism for triplet excited state decay: combined spin-orbit and nonadiabatic couplings. J. Chem. Theor. Comput. 9 (2), 1132—1143. https://doi.org/10.1021/ct300798t.

Peng, Q., Yi, Y., Shuai, Z.G., Shao, J., 2007. Toward quantitative prediction of molecular fluorescence quantum efficiency: role of Duschinsky rotation. J. Am. Chem. Soc. 129 (30), 9333—9339. https://doi.org/10.1021/ja067946e.

Qu, R., Li, C., Liu, J., Xiao, R., Pan, X., Zeng, X., Wu, J., 2018. Hydroxyl radical based photocatalytic degradation of halogenated organic contaminants and paraffin on silica gel. Environ. Sci. Technol. 52 (13), 7220—7229. https://doi.org/10.1021/acs.est.8b00499.

Raghavachari, K., Binkley, J.S., Seeger, R., Pople, J.A., 1980. Self-consistent molecular orbital methods. 20. Basis set for correlated wave-functions. J. Chem. Phys. 72 (1), 650—654. https://doi.org/10.1063/1.438955.

Segura, P.A., Francois, M., Gagnon, C., Sauve, S., 2009. Review of the occurrence of anti-infectives in contaminated wastewaters and natural and drinking waters. Environ. Health Perspect. 117 (5), 675—684. https://doi.org/10.1289/ehp.11776.

Serna-Galvis, E.A., Ferraro, F., Silva-Agredo, J., Torres-Palma, R.A., 2017. Degradation of highly consumed fluoroquinolones, penicillins and cephalosporins in distilled water and simulated hospital wastewater by UV254 and UV254/persulfate processes. Water Res. 122, 128—138. https://doi.org/10.1016/j.watres.2017.05.065.

Shah, S.Q.A., Colquhoun, D.J., Nikuli, H.L., Sørum, H., 2012. Prevalence of antibiotic resistance genes in the bacterial flora of integrated fish farming environments of Pakistan and Tanzania. Environ. Sci. Technol. 46 (16), 8672—8679. https://doi.org/10.1021/es3018607.

Stoll, C., Sidhu, J.P.S., Tiehm, A., Toze, S., 2012. Prevalence of clinically relevant antibiotic resistance genes in surface water samples collected from Germany and Australia. Environ. Sci. Technol. 46 (17), 9716—9726. https://doi.org/10.1021/es302020s.

Sturini, M., Speltini, A., Maraschi, F., Profumo, A., Pretali, L., Fasani, E., Albini, A., 2010. Photochemical degradation of marbofloxacin and enrofloxacin in natural waters. Environ. Sci. Technol. 44 (12), 4564—4569. https://doi.org/10.1021/es100278n.

Tentscher, P.R., Eustis, S.N., McNeill, K., Arey, J.S., 2013. Aqueous oxidation of sulfonamide antibiotics: aromatic nucleophilic substitution of an aniline radical cation. Chem. Eur J. 19, 11216—11223. https://doi.org/10.1002/chem.201204005.

te Velde, G., Bickelhaupt, F.M., van Gisbergen, S.J.A., Fonseca Guerra, C., Baerends, E.J., Snijders, J.G., Ziegler, T., 2001. Chemistry with ADF. J. Comput. Chem. 22 (9), 931—967. https://doi.org/10.1002/jcc.1056.

Tomasi, J., Mennucci, B., Cammi, R., 2005. Quantum mechanical continuum solvation models. Chem. Rev. 105 (8), 2999—3093. https://doi.org/10.1021/cr9904009.

Turel, I., 2002. The interactions of metal ions with quinolone antibacterial agents. Coord. Chem. Rev. 232 (1—2), 27—47. https://doi.org/10.1016/S0010-8545(02)00027-9.

van Lenthe, E., Baerends, E.J., Snijders, J.G., 1994. Relativistic total energy using regular approximations. J. Chem. Phys. 101 (11), 9783—9792. https://doi.org/10.1063/1.467943.

van Lenthe, E., Ehlers, A.E., Baerends, E.J., 1999. Geometry optimization in the zero order regular approximation for relativistic effects. J. Chem. Phys. 110 (18), 8943—8953. https://doi.org/10.1063/1.478813.

van Lenthe, E., Snijders, J.G., Baerends, E.J., 1996a. The zero-order regular approximation for relativistic effects: the effect of spin-orbit coupling in closed shell molecules. J. Chem. Phys. 105 (15), 6505—6516. https://doi.org/10.1063/1.472460.

van Lenthe, E., Van Leeuwen, R., Baerends, E.J., Snijders, J.G., 1993. Relativistic regular 2-component Hamiltonians. J. Chem. Phys. 99 (6), 4597—4610. https://doi.org/10.1063/1.466059.

van Lenthe, E., Van Leeuwen, R., Baerends, E.J., Snijders, J.G., 1996b. Relativistic regular two-component Hamiltonians. Int. J. Quant. Chem. 57 (3), 281—293. https://doi.org/10.1002/(SICI)1097-461X(1996)57:3<281::AID-QUA2>3.0.CO;2-U.

Wammer, K.H., Korte, A.R., Lundeen, R.A., Sundberg, J.E., McNeill, K., Arnold, W.A., 2013. Direct photochemistry of three fluoroquinolone antibacterials: norfloxacin, ofloxacin, and enrofloxacin. Water Res. 47, 439—448. https://doi.org/10.1016/j.watres.2012.10.025.

Wang, S., Song, X., Hao, C., Gao, Z., Chen, J., Qiu, J., 2015. Elucidating triplet-sensitized photolysis mechanisms of sulfadiazine and metal ions effects by quantum chemical calculations. Chemosphere 122, 62—69. https://doi.org/10.1016/j.chemosphere.2014.11.007.

Wei, X., Chen, J., Xie, Q., Zhang, S., Ge, L., Qiao, X., 2013. Distinct photolytic mechanisms and products for different dissociation species of ciprofloxacin. Environ. Sci. Technol. 47, 4284—4290. https://doi.org/10.1021/es400425b.

Werner, J.J., Arnold, W.A., McNeill, K., 2006. Water hardness as a photochemical parameter: tetracycline photolysis as a function of calcium concentration, magnesium concentration, and pH. Environ. Sci. Technol. 44, 2400—2405. https://doi.org/10.1021/es060337m.

Zeng, X., Qu, R., Feng, M., Chen, J., Wang, L., Wang, Z., 2016. Photodegradation of polyfluorinated dibenzo-p-dioxins in organic solvents: experimental and theoretical studies. Environ. Sci. Technol. 50 (15), 8128—8134. https://doi.org/10.1021/acs.est.6b02682.

Zhang, T., Jiang, Y., Niu, Y.L., Wang, D., Peng, Q., Shuai, Z.G., 2014. Aggregation effects on the optical emission of 1,1,2,3,4,5-Hexaphenylsilole (HPS): a QM/MM Study. J. Phys. Chem. 118, 9094—9104. https://doi.org/10.1021/jp5021017.

Zhang, Q.Q., Ying, G.G., Pan, C.G., Liu, Y.S., Zhao, J.L., 2015. Comprehensive evaluation of antibiotics emission and fate in the river basins of China: source analysis, multimedia modeling, and linkage to bacterial resistance. Environ. Sci. Technol. 49, 6772—6782. https://doi.org/10.1021/acs.est.5b00729.

Zhang, Z.C., Xie, X.D., Yu, Z.Q., Cheng, H.F., 2019. Influence of chemical speciation on photochemical transformation of three fluoroquinolones (FQs) in water: kinetics, mechanism, and toxicity of photolysis products. Water Res. 148, 19—29. https://doi.org/10.1016/j.watres.2018.10.027.

Zhu, Z., Lu, Z., Wang, D., Tang, X., Yan, Y., Shi, W., Wang, Y., Gao, N., Yao, X., Dong, H., 2016. Construction of high-dispersed Ag/Fe3O4/g-C3N4 photocatalyst by selective photo-deposition and improved photocatalytic activity. Appl. Catal., B 182, 115—122. https://doi.org/10.1016/j.apcatb.2015.09.029.